Constrained Warping of Thin-Walled Hollow Composite Beams

Cheol Kim* and Scott R. White†
University of Illinois at Urbana–Champaign, Urbana, Illinois 61801

Introduction

EXTENSIVE research has been done over the past decade on composite thin-walled beam theories that account for coupling responses and torsional warping.[1–4] Torsional warping is significant for thin-walled composite beams with closed and open cross sections, so that most beam analyses include the effects of free warping (St. Venant torsion). However, constrained warping (Vlasov torsion) tends to be considered only in the analysis of composite beams with open sections such as I beams. This results by inference from the well-known fact that torsional warping of isotropic beams with closed cross sections is much smaller than that with open cross sections. Because of the complex structural couplings of composite beams, constrained warping may not always be negligible for closed sections.

Analytical Formulation

The beam displacements can be expressed as

$$u(x,s,n) = u_o(x) - r_y\left\{\phi_y(x) + \left(r_y\frac{d_2-d_1}{d_1d_2} + \frac{4r_y^2}{3d_1d_2}\right)\times[v_o'(x) - \phi_y(x)]\right\} - r_z\left\{\phi_z(x) + \left(r_z\frac{c_2-c_1}{c_1c_2} + \frac{4r_z^2}{3c_1c_2}\right)\times[w_o'(x) - \phi_z(x)]\right\} - \psi_c(x,s)\theta'(x) \tag{1a}$$

$$u_s(x,s,n) = v_o(x)\frac{d\bar{y}(s)}{ds} + w_o(x)\frac{d\bar{z}(s)}{ds} + \theta(x)[r_n(s)+n] \tag{1b}$$

$$u_n(x,s,n) = v_o(x)\frac{d\bar{z}(s)}{ds} - w_o(x)\frac{d\bar{y}(s)}{ds} - \theta(x)r_s(s) \tag{1c}$$

where the functions u_s, u_n, and u are the curvilinear tangential, normal, and axial displacements, respectively. The functions $u_o(x)$, $v_o(x)$, and $w_o(x)$ represent the rigid body translations along the x, y, and z axes, respectively; the variables $\phi_y(x)$ and $\phi_z(x)$ denote the rotations about the z and y axes, respectively; and $\theta(x)$ is the angle of twist. The function $\psi_c(x,s)$ denotes the constrained warping. The equations $y = \bar{y}(s)$ and $z = \bar{z}(s)$ define the midline contour in the beam cross section, and the prime denotes differentiation with respect to x. The functions r_s and r_n are defined as

$$r_s(s) = \bar{y}(s)\frac{d\bar{y}(s)}{ds} + \bar{z}(s)\frac{d\bar{z}(s)}{ds} \qquad r_n(s) = \bar{y}(s)\frac{d\bar{z}(s)}{ds} - \bar{z}(s)\frac{d\bar{y}(s)}{ds} \tag{2}$$

The functions r_y and r_z denote the y and z components of the position vector $\boldsymbol{r}$ in Fig. 1, respectively.

A constrained torsional warping function can be written as[4,5]

$$\psi_c(x,s) = (2AD_1/\Omega)\varphi(s)[\tanh\lambda L\sinh\lambda x - \cosh\lambda x + 1] \tag{3a}$$

$$= \psi_f(s)[\tanh\lambda L\sinh\lambda x - \cosh\lambda x + 1] \tag{3b}$$

where

$$A = \frac{1}{2}\oint r_n(\tau)\,d\tau \qquad \Omega = \oint\frac{d\tau}{B_{xs}(\tau)} \tag{4a}$$

$$D_1 = \oint\frac{\Gamma(\tau)}{B_{xs}(\tau)}\,d\tau \qquad D_2 = \oint\frac{\Gamma^2(\tau)}{B_{xs}(\tau)}\,d\tau \tag{4b}$$

$$\Gamma(s) = \frac{1}{D_\phi}\left[\frac{1}{2A}\oint\Lambda(\tau)r_n\,d\tau - \Lambda(s)\right] \tag{4c}$$

$$\Lambda(s) = \int_o^s B_{xx}(\tau)\varphi(\tau)\,d\tau \qquad D_\phi = \oint B_{xx}(\tau)\varphi^2(\tau)\,d\tau \tag{4d}$$

$$\lambda = (D_\phi D_2)^{-\frac{1}{2}} \qquad \varphi(s) = \bar{y}(s)\bar{z}(s) \tag{4e}$$

and $B_{xx}(s) = E_e(s)h(s)$, $B_{xs}(s) = G_e(s)h(s)$, and $E_e(s)$ and $G_e(s)$ are the effective longitudinal and shear moduli, respectively. The variable $\psi_f(s)$ is the free torsional warping function and is independent of the beam axial coordinate x. From Eq. (3b), the constrained warping effect is seen to be governed by the warping decay parameter λ. The resulting strains are obtained by using linear strain-displacement relations. The reduced constitutive equations with three-dimensional elastic effects for a single layer and the equilibrium equations acting over the cross section can be found in Ref. 4.

Torsional Warping Effects

Consider the torsional warping behavior of a cantilever thin-walled composite rectangular section beam tightly fixed at the support where additional torsional rigidity is introduced because of the constrained warping. The constrained warping function can be readily determined by integrating Eqs. (4) along the beam contour:

$$\psi_c(x,y,z) = \kappa(\tanh\lambda L\sinh\lambda x - \cosh\lambda x + 1)yz \tag{5}$$

where

$$\kappa = (\zeta-1)/(\zeta+1) \qquad \zeta = (d/c)(h_v/h_h)(G_{ev}/G_{eh}) \tag{6}$$

The subscripts h and v denote horizontal and vertical walls, respectively.

The influence of geometry and material on the torsional behavior of the beam are sensed through the parameter λ. A large value of λ implies rapid decay of the constrained warping effect along the beam span. The warping decay parameter can be expressed as

$$\lambda^{-2} = \left[\frac{9(d^3+5cd^2)B_{xx}^{h^2} + 5(c^2d+5c^3)B_{xx}^{v^2} + 10(9c^2d+cd^2)B_{xx}^hB_{xx}^v}{240B_{xs}^h} - \frac{10cd^2B_{xx}^{h^2} + 9c^3B_{xx}^{v^2} + 20c^2dB_{xx}^hB_{xx}^v}{60B_{xs}^v}\right]\frac{1}{dB_{xx}^h + cB_{xx}^v} \tag{7}$$

where

$$B_{xx}^h = E_{eh}\times h_h \qquad B_{xx}^v = E_{ev}\times h_v$$

$$B_{xs}^h = G_{eh}\times h_h \qquad B_{xs}^v = G_{ev}\times h_v$$

If the material is isotropic, Eq. (7) reduces to

$$\lambda^2 = \frac{80}{(3d^2+2dc+3c^2)}\times\frac{G}{E} \tag{8}$$

which is close to Benscoter's[6] approximate torsion theory, $\lambda^2 = [48/(d+c)^2](G/E)$.

To evaluate the influence of λ on the torsional behavior of composite beams, the torsional warping is expressed in terms of relative torsional warping ($\Delta\omega$), which is the ratio of the constrained torsional warping to the free warping, so that

$$\Delta\omega = \tanh\lambda L\sinh\lambda x - \cosh\lambda x + 1 \tag{9}$$

Received Aug. 1, 1995; revision received Jan. 29, 1997; accepted for publication March 14, 1997.

*Postdoctoral Research Associate, Department of Aeronautical and Astronautical Engineering; currently Senior Researcher, Samsung Aerospace R&D Center, Daejon 305-340, Republic of Korea. Member AIAA.

†Associate Professor, Department of Aeronautical and Astronautical Engineering. Member AIAA.

The length of the warping restrained region (critical region) can be expressed as $\Delta\omega < 1.0$. Solving Eq. (9) when $\Delta\omega = 1$ gives the length of the critical region

$$x_{cr} = \frac{1}{\lambda}\tanh^{-1}\left(\frac{1}{\tanh \lambda L}\right) \tag{10}$$

Beyond x_{cr}, the composite beam is considered to be under St. Venant torsion. The critical length depends on both the geometry and the mechanical properties of the composite beam.

Examples

To assess the constrained warping effects, cantilever hollow rectangular beams consisting of aluminum and graphite/epoxy are considered in this Note (Fig. 1). Their mechanical properties and geometric parameters are given in Tables 1 and 2. The nondimensional warping decay parameter λL and critical length x_{cr} for beam A with several layup sequences are summarized in Table 3. Circumferentially asymmetric stiffness (CAS) beams produce a bending-twist coupling so that an applied bending moment or torque produces a coupled deflection and twisting. From Table 3, it is apparent that all of the composite beams have larger critical lengths compared to the isotropic beam. This indicates that the constrained warping effects are more significant for composite beams than for isotropic beams. To see the effect of the slenderness ratio on torsional warping, the length of the CAS1 beam A was kept constant and the width d and depth c were increased proportionally so that the slenderness ratio changes. As the slenderness ratio increases, the effects of constrained warping are mitigated. For a slenderness ratio of 8.0, over 50% of beam length is under the influence of constrained warping, whereas for a slenderness ratio of 34, only 10% of the beam is constrained.

To investigate the influence of constrained torsional warping on global beam deformations, beams A and B with a CAS1 layup sequence are considered. The values of λL are 24.96 for beam A and 6.24 for beam B. Figure 2 shows the bending-inducedtwist angle of beam A subjected to a 4.45-N tip shear load at the geometric center. Here, constrained warping accounts for a difference of 4% in the tip twist angle compared to free warping. The free warping test data[1] are also plotted for comparison. It can be seen that the constrained warping effect is small for this slender beam. On the other hand, the constraint effect is more pronounced for beams with lower slenderness ratios. For beam B (low slenderness ratio) acted upon by a 0.113-N ·m tip torque, the reduction in bending-inducedtwist at the tip of the beam is 13%, as shown in Fig. 3. This reduction is large enough to invalidate the assumption of purely St. Venant torsional behavior.

Constrained warping can also lead to significant elevation of stresses within the affected regions. The normal and shear stress resultants (N_{xx} and N_{xs}) were calculated for beam B with the CAS1 layup subjected to a 0.113-N ·m tip torque. The maximum shear stress resultant occurs at the cantilevered end ($x = 0$) at $z = 0$ and is 26% higher than the shear flow ($q = T/2A$) because of free warping, i.e., $(N_{xs})_{max}/q = 1.26$. The maximum normal stress resultant occurs at the corners of the box beam at the cantilevered end. In the flange region $[(N_{xx})_{max}/q]|_{flange} = 1.30$, and in the web region $[(N_{xx})_{max}/q]|_{web} = 2.43$.

In light of the complex structural couplings of composite hollow beams, as demonstrated in the preceding examples, the influence of constrained warping may be significant, depending on wall layup

Table 1 Mechanical properties of aluminum and graphite/epoxy

Aluminum (isotropic)	
$E = 71.0$ GPa	$G = 26.2$ GPa
$\nu = 0.3$	
AS4/3501-6 (graphite/epoxy)	
$E_{11} = 141.96$ GPa	$E_{22} = E_{33} = 9.79$ GPa
$G_{12} = G_{13} = 6.0$ GPa	$G_{23} = 4.83$ GPa
$\nu_{12} = \nu_{13} = 0.3$	$\nu_{23} = 0.43$

Table 2 Thin-walled rectangular beam geometry

Parameters	Beam A	Beam B
Length L, mm	762.0	762.0
Outer width d, mm	24.2	96.8
Outer depth c, mm	13.6	54.5
Slenderness ratio L/d	31.5	8.0
Wall thickness h, mm	0.762	0.762
Number of layers	6	6
Layer thickness, mm	0.127	0.127

Table 3 Decaying parameters and critical length for different layups

Materials	Flanges	Webs	λL	x_{cr}/L, %
Aluminum			75.88	8.0
Graphite/epoxy				
Cross-ply	$[0/90]_3$	$[0/90]_3$	34.11	17.9
CAS1	$[15]_6$	$[+15/-15]_3$	24.96	24.5
CAS2	$[30]_6$	$[+30/-30]_3$	39.72	15.4
CAS3	$[45]_6$	$[+45/-45]_3$	59.94	10.2

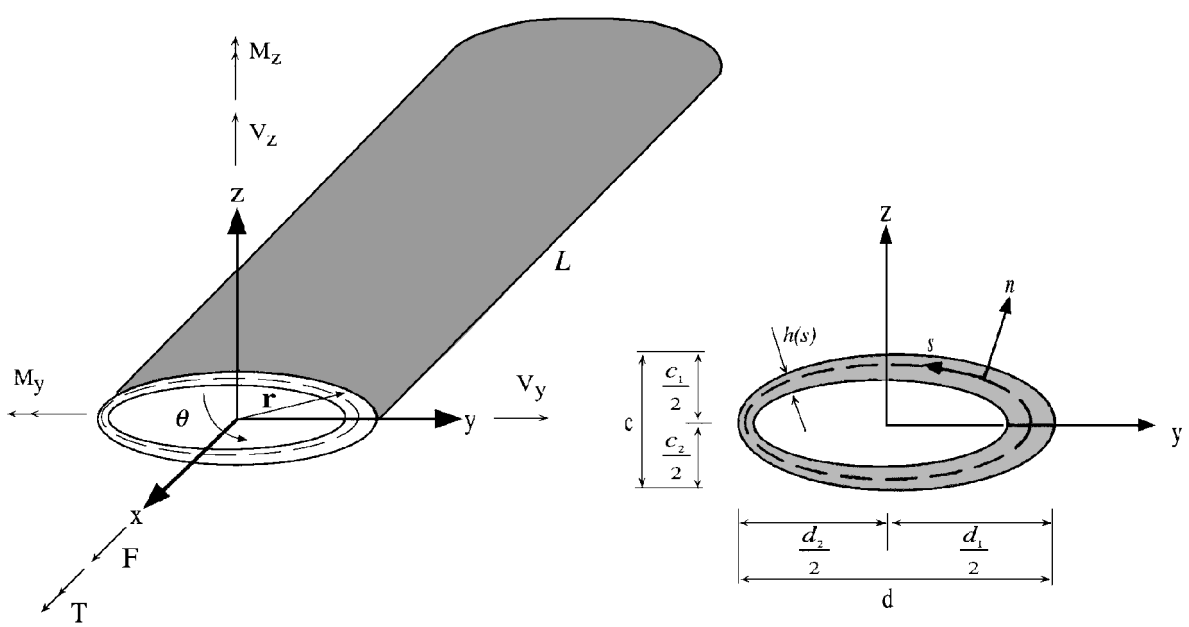

Fig. 1 Coordinate systems and geometry of a closed section beam.

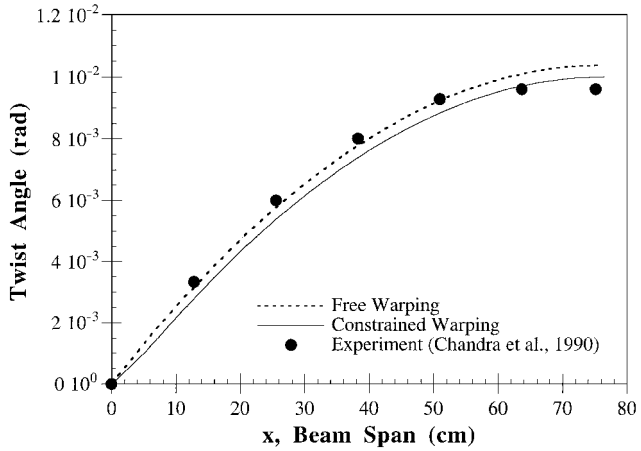

Fig. 2 Bending-induced twist angle of CAS1 beam A acted upon by 4.45-N tip shear load.

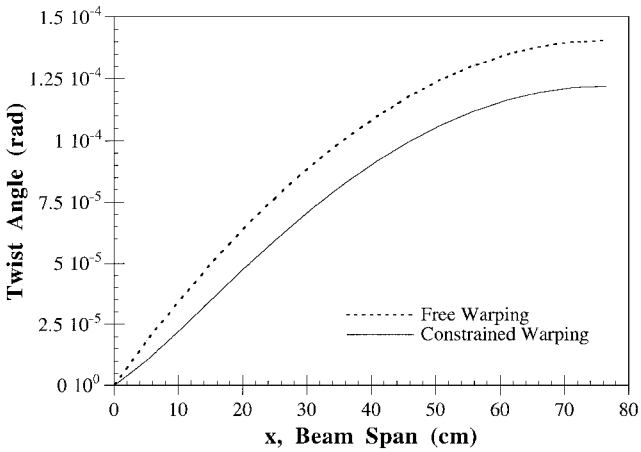

Fig. 3 Bending-induced twist angle of CAS1 beam B acted upon by 4.45-N tip shear load.

sequences, induced deformations, and slenderness ratio. Neglecting this effect by using a St. Venant torsional analysis can give erroneous results and significant underprediction of stresses in some cases.

Conclusions

The constrained warping effect is found to be significant enough to be included in the analysis of composite hollow beams in certain circumstances. A small nondimensional warping decay parameter (λL) gives a large critical length of constrained warping (x_{cr}). This length depends on the geometry and the mechanical properties of the beam. Larger x_{cr} of composite hollow beams compared to isotropic hollow beams indicates that constrained warping in composites is of more significance. A large slenderness ratio tends to mitigate the effects of constrained warping. In one of the examples (slenderness ratio = 8, $\lambda L = 25$), the bending-induced twist angle was shown to be reduced by 13% because of the constraint effect. Additional stresses caused by constrained warping can be very high. An example shows that maximum N_{xs} and N_{xx} at the support are higher by 26 and 143% than free warping.

References

[1]Chandra, R., Stemple, A. D., and Chopra, I., "Thin-Walled Composite Beams Under Bending, Torsional, and Extensional Loads," *Journal of Aircraft*, Vol. 27, No. 7, 1990, pp. 619–626.

[2]Berdichevsky, V., Armanios, E., and Badir, A., "Theory of Anisotropic Thin-Walled Closed-Cross-Section Beams," *Composite Engineering*, Vol. 2, Nos. 5–7, 1992, pp. 411–432.

[3]Rehfield, L. W., Atilgan, A. R., and Hodges, D. H., "Nonclassical Behavior of Thin-Walled Composite Beams with Closed Cross Sections," *Journal of the American Helicopter Society*, Vol. 35, No. 2, 1990, pp. 42–50.

[4]Kim, C., and White, S. R., "Analysis of Thick Hollow Composite Beams Under General Loadings," *Composite Structures*, Vol. 34, 1996, pp. 263–277.

[5]Vasiliev, V. V., *Mechanics of Composite Structures*, Taylor and Francis, Washington, DC, 1993.

[6]Benscoter, S. U., "A Theory of Torsion Bending for Multicell Beams," *Journal of Applied Mechanics*, Vol. 21, No. 1, 1954, pp. 25–34.

R. K. Kapania
Associate Editor

Convergence of Methods for Nonlinear Eigenvalue Problems

Per Bäck* and Ulf Ringertz†
Royal Institute of Technology, S-100 44 Stockholm, Sweden

Nomenclature

$\boldsymbol{A}$ = matrix of aerodynamic forces
b = semichord
$\boldsymbol{K}$ = stiffness matrix
k = reduced frequency, $\omega b/u$
M = Mach number
$\boldsymbol{M}$ = consistent mass matrix
p = eigenvalue
q = dynamic pressure, $\rho u^2/2$
$\hat{q}$ = nondimensional dynamic pressure; $\hat{q} \in (0, 1)$
u = airspeed
$\tilde{\boldsymbol{v}}$ = eigenvector
ρ = air density
$\boldsymbol{\Omega}$ = diagonal matrix with free vibration frequencies
ω = vibration frequency

Introduction

ALTHOUGH significant advances have been made in the use of nonlinear fluid mechanics models for aeroelasticity analysis,[1] most analysis is still performed using linear unsteady potential flow models. Combining linear elastic structural dynamics with linear unsteady potential flow, it is possible to analyze the stability of quite complex aircraft structures by solving a nonlinear eigenvalue problem. There are several different methods available for the solution of nonlinear eigenvalue problems,[2] and this Note focuses on the convergence properties of a particular method known as the p–k method.

Assuming linear structural dynamics, the equations of motion for an aircraft wing structure may be given in discretized form as

$$\boldsymbol{M}\ddot{\boldsymbol{v}} + \boldsymbol{K}\boldsymbol{v} = \boldsymbol{f}(t) \tag{1}$$

where the vector $\boldsymbol{v} \in R^n$ denotes the nodal displacements of the wing finite element model.

Assuming linear unsteady aerodynamics and transforming the equations to the frequency domain gives the eigenvalue problem

$$[p^2\boldsymbol{M} + \boldsymbol{K} - q\boldsymbol{A}(M, p)]\tilde{\boldsymbol{v}} = 0 \tag{2}$$

Following standard procedures,[2] the eigenvalue problem is transformed using a modal subspace into the nondimensional form given by

$$[\hat{p}^2\boldsymbol{I} + \boldsymbol{\Omega}^2 - \hat{q}\hat{\boldsymbol{A}}(\hat{p}, M)]\hat{\boldsymbol{v}} = 0 \tag{3}$$

where $\hat{\boldsymbol{v}} \in R^m$ and usually with $m \ll n$. The nondimensional eigenvalue $\hat{p}$ is defined such that the imaginary part equals the reduced frequency k.

Received June 25, 1996; revision received Jan. 31, 1997; accepted for publication March 17, 1997.

*Graduate Student, Department of Aeronautics.
†Associate Professor, Department of Aeronautics. Member AIAA.